Robust Wave-front Correction in a Small-Scale Adaptive Optics System Using a Membrane Deformable Mirror

Seung-Kyu Park and Sung-Hoon Baik
Korea Atomic Energy Research Institute, 1045 Daedeokdaero, Yuseong-gu, Daejeon 305-353, Republic of Korea
Jong Kyu Jung and Soo Man Lee
Optoelectronic System Development Center, Doosan DST, Republic of Korea
Jaeeun Yoo and Young Soo Choi
Agency for Defense Development, Daejeon, Republic of Korea

ABSTRACT

A small-scale laboratory adaptive optics system using a Shack-Hartmann wave-front sensor (WFS) and a membrane deformable mirror (DM) has been built for robust image acquisition. In this study, an adaptive limited control technique is devised to maintain the long-term correction stability of the adaptive optics system. To prevent the waste of dynamic correction range for small residual wave-front distortions, which are inefficient to correct, the developed system tries to limit wave-front corrections when a similar small difference in the wave-front pattern is repeatedly generated. In addition, the effect of mechanical distortion in an adaptive optics system is studied and a pre-recognition method for the distortion is devised to keep the optimal performance over a long period of time. A confirmation process for a balanced work assignment among deformable mirror (DM) actuators is adopted for the pre-recognition. The corrected experimental results obtained by using a built small scale adaptive optics system are described in this paper.

1. INTRODUCTION

Wave-front control is a widely-used technique to improve the performance of optical systems by actively correcting wave-front distortions due to atmospheric turbulence, optical fabrication errors, thermal effects, and laser or laser device aberrations [1-3]. The principal applications of wave-front control are improving the image quality in optical imaging systems such as infrared astronomical telescopes, imaging, and tracking rapidly moving space objects, and compensating for laser beam distortion through the atmosphere [4-7]. Nowadays, an adaptive optics technique for wave-front correction, combined with OCT (optical coherence tomography), is widely used to improve the image quality of an in-vivo human retina [7-9]

A conventional adaptive optics system consists of a wave-front sensor, a deformable mirror (DM), and a control computer. The control computer measures the wave-front distortion by using a wave-front sensor and corrects it by using a deformable mirror in a closed-loop. The key factors in a closed-loop adaptive optics system are the correction efficiency and system stability [10-11]. The performance of an adaptive optics system depends highly on the correction capability of the deformable mirror, which is comparatively expensive among the configuration components of an adaptive optics system. Thus, an economical configuration of a system using a cost-effective deformable mirror is essential for expansion to industrial applications. In addition, the stabilization of the configured system is a key in practical applications. Suppression for high-order Eigen modes in the influence function matrix of a DM is conventionally used to improve the stabilization. The technique improves the system's stability by widening the dynamic range of the DM's actuators, but it decreases the accuracy of the correction capability. The correction efficiency of the system is also decreased if the mechanical arrangement between a wave-front sensor and a corrector is distorted. The distortion decreases the system performance because it reduces the dynamic correction range of the system. Thus, users may run a system with its low-performance if they do not recognize the arrangement distortion.

In this study, a stabilization technique without a decrease in the correction accuracy of the built adaptive optics system using a cost-effective membrane deformable mirror was investigated. An adaptive limited correction method was devised to improve the stability of the system by not using voltage resources to correct small non-effective distortions. The effect of mechanical distortion in an adaptive optics system using a Shack-Hartmann wave-front sensor (SHS) and an economical membrane deformable mirror (DM) is also studied, and a pre-recognition method

for the mechanical distortion is then investigated to prevent the system from running at a low-performance level. An inspection process for a balanced work assignment among the DM actuators is adopted to recognize the mechanical distortion. The technique for confirming balanced eigenvalues can provide optimal arrangement information of an adaptive optics system. Correction experiments using the stabilization and confirmation techniques are carried out, and the experimental results are compared in this manuscript.

2. CONFIGURATION OF A BUILT SMALL SCALE ADAPTIVE OPTICS SYSTEM

A block-diagram of the built adaptive optics system is shown in Fig. 1, and a photo is shown in Fig. 2. The closed-loop adaptive optics system consists of a tip/tilt sensor (TTC: acA640-100gm, Basler Inc.), a Shack-Hartmann-type wave-front sensor (WFS: WFS10-14AR, Thorlabs Inc.), a membrane deformable mirror (DM: MultiDM140-35, Boston Micromachines), a tip/tilt mirror (TTM: S-340.SSL, PI Co.), a monitoring camera for Strehl-ratio (SC: acA640-120gm, Basler Inc.), an image acquisition camera (IC: acA640-120gm, Basler Inc.), and a control computer (PC, CPU-I7, Windows).

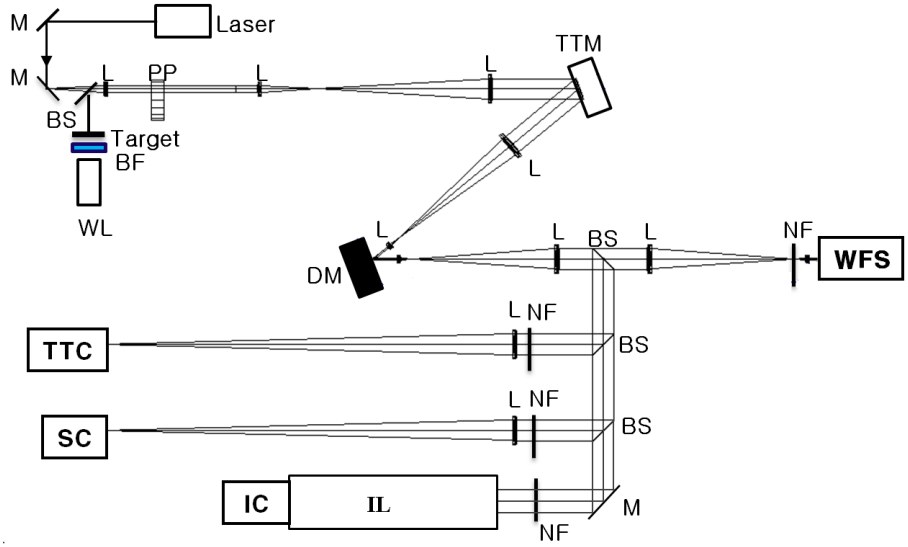

Fig. 1. Block diagram of the developed small-scale adaptive optics system.

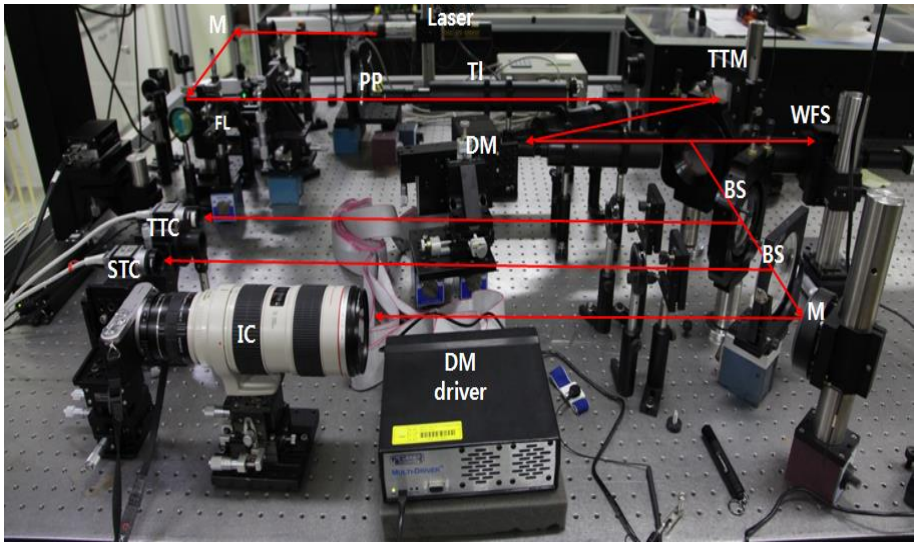

Fig. 2. Photograph of the developed small-scale adaptive optics system.

As shown in Fig. 1, a wave-front image is acquired by a Shack-Hartmann-type wave-front sensor (WFS) after the He-Ne laser beam passes through a phase plate (PP, Lexitek Inc.), a tilt mirror (TTM), and a deformable mirror (DM). The data of the wave-front error are calculated by extracting the moved center positions of the X-axis and Y-axis for a local wave-front spot image in each sub-aperture. Tilt data of the X-axis and the Y-axis are acquired by the TTC. Here, the tilt data are calculated by extracting the movement of a focused laser spot image. The wave-front slope and the tilt data are calculated by acquiring the centroid's movement of each spot image. The control computer then corrects for the tilt error using a tip/tilt mirror (TTM), and corrects for the wave-front errors using a deformable mirror (DM) after calculating the correction voltages in modal or zonal control mode. In Figs. 1 and 2, the notation M indicates a mirror, L is a lens, BS is a beam splitter, NF is a neutral density filter, and IL is the imaging optics. A rotating phase plate (PP) is used to artificially produce wave-front distortions. One camera (SC) is used for monitoring the Strehl-ratio of the laser beam in real-time and another image camera (IC) is used for observing the real-time image.

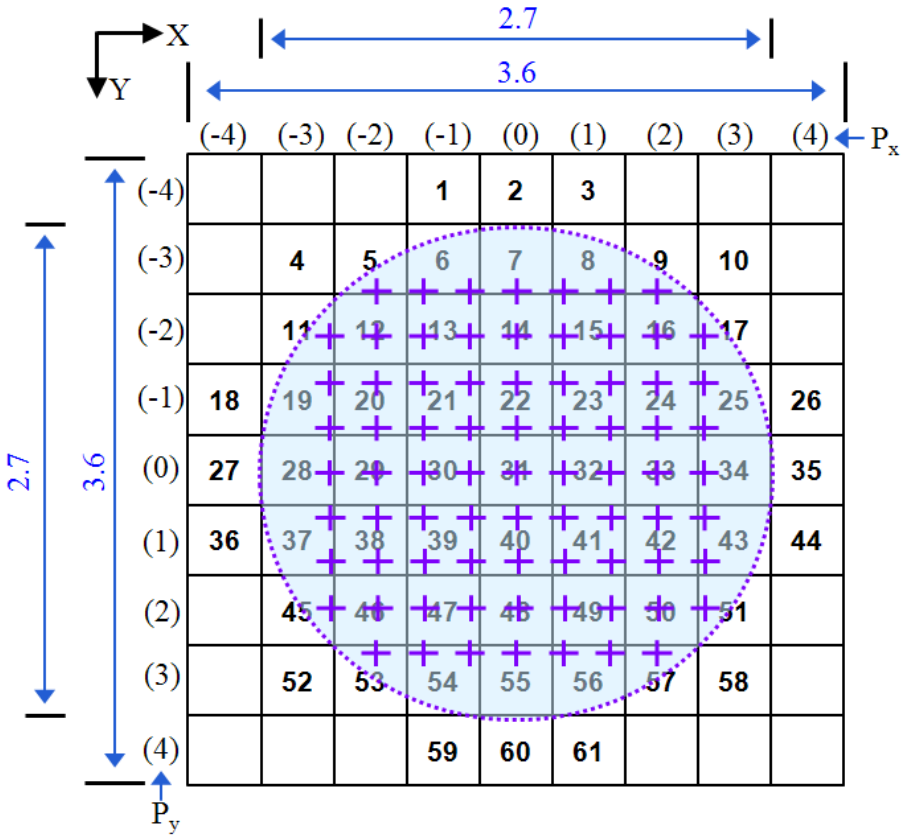

Fig. 3. Arrangement of a wave-front sensor and a deformable mirror.

The configured position map between the WFS and DM is shown in Fig. 3. It is a conventional position map, where the integer is the actuator number of the DM, and the notation '+' indicates the center position of each sub-aperture in the WFS. Here, the center position '+' shows the total sub-apertures of a reference wave-front supplied by the WFS manufacturer. The sizes of the DM and WFS are about 3.6 mm x 3.6 mm and 2.7 mm x 2.7 mm, respectively.

Two-dimensional (2D) and three-dimensional (3D) images of a non-corrected wave-front image are shown in Figs. 4(a) and 4(b), respectively. Corrected 2D and 3D wave-front images after the corrections are shown in Fig. 5(a) and Fig. 5(b), respectively.

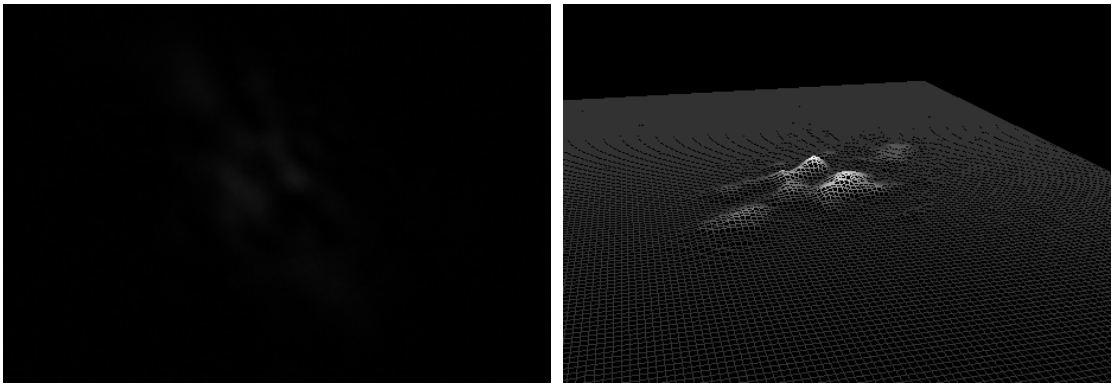

(a) 2D image (b) 3D image

Fig. 4. Images of a laser beam before wave-front correction.

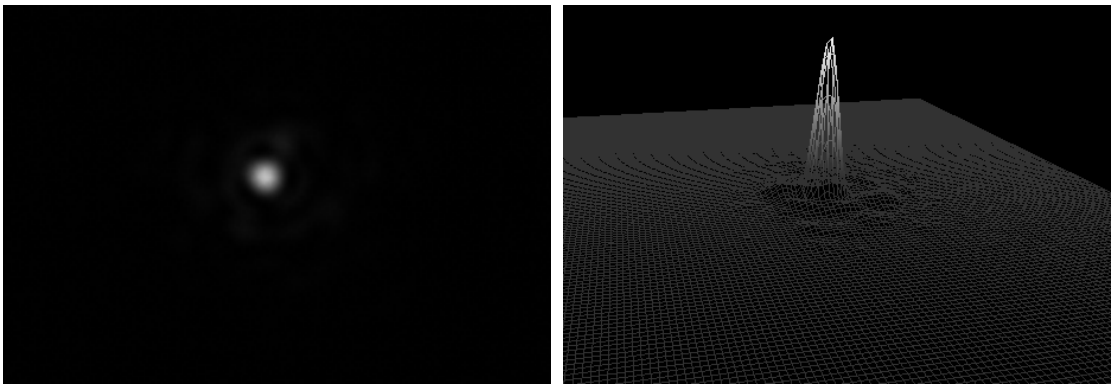

(a) 2D image (b) 3D image

Fig. 5. Images of a laser beam after the wave-front correction.

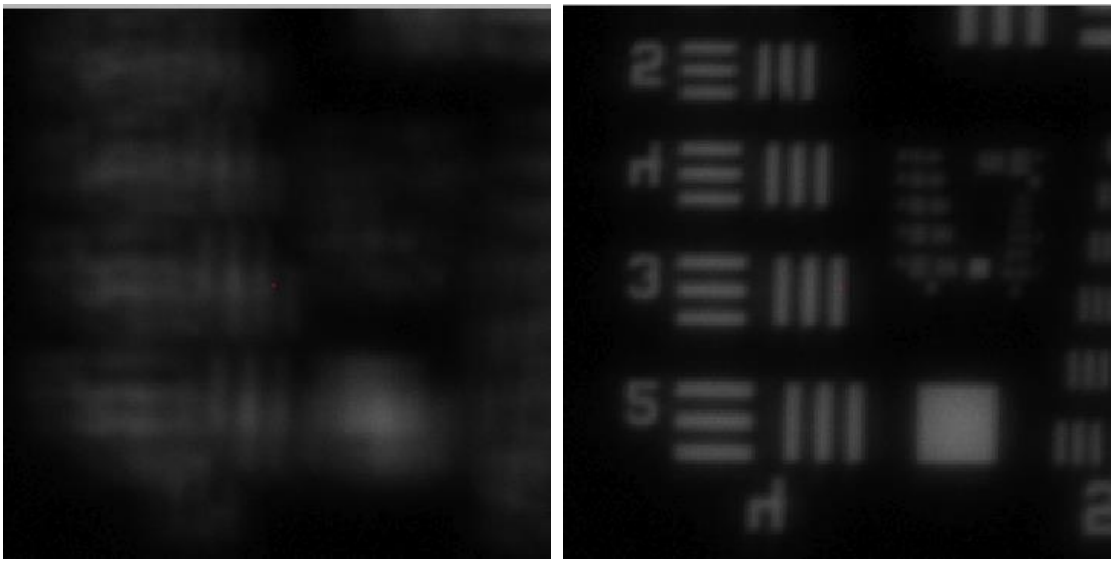

(a) Before correction (b) After correction

Fig. 6. Image comparison of before (a) and after (a) correction for wave-front distortion.

The system corrects for the wave-front error generated by a rotating phase plate in a closed-loop. The correction speed of the system varied within the range of 60 to 120 Hz. For the experiments, the rotating speed of the phase plate having an atmospheric coherence length of 15 cm was 3.7 mm/s, which corresponds to a wind speed of 0.5

m/s. The range of the Strehl ratio for the corrected wave-front was improved to about 0.4 to 0.7 from the non-corrected ratio of 0.07 to 0.3. The monitored IC sample images before and after the wave-front corrections are shown in Fig. 6 (a) and Fig. 6(b), respectively.

3. EXPERIMENTS FOR ROBUST WAVE-FRONT CORRECTION USING A BUILT SMALL SCALE ADAPTIVE OPTICS SYSTEM

The long-term stability of an adaptive optics system is essential for practical field applications. The dynamic range of a closed-loop wave-front correction control system is decreased when the system consumes its voltage resources to correct for small residual distortions. In principle, an adaptive optics system tries to correct for all the current wave-front distortions measured by a sensor. If the system tries to correct for small uncorrectable distortions or small systematic residual distortions, the system wastes its capability; thus, its control dynamic range is decreased. The voltage values of the DM actuators in a configured closed-loop system can be saturated within sub-seconds if the DM tries to correct for small, non-meaningful and uncorrectable distortions.
The saturated voltages according to the number of corrections for actuators 5, 28, and 60 are shown in Fig. 7(a). Here, the rotating phase plate was stopped to make a fixed wave-front distortion. According to the number of corrections, the peak-to-valley (PV) value and root-mean-square (RMS) value of the Zernike coefficients from 1 to 36 are shown in Fig. 7(b). Although the built adaptive optics system looked like it was correcting for the wave-front distortion well, as shown in Fig. 7(b), the system consumed voltage resources to correct for small wave-front distortions. When we checked the voltages of the three actuators (5, 28, 60), we found they were saturated after the 47^{th}, 111^{th}, and 618^{th} corrections. These actuators were not used for the correction of the next wave-front distortion.

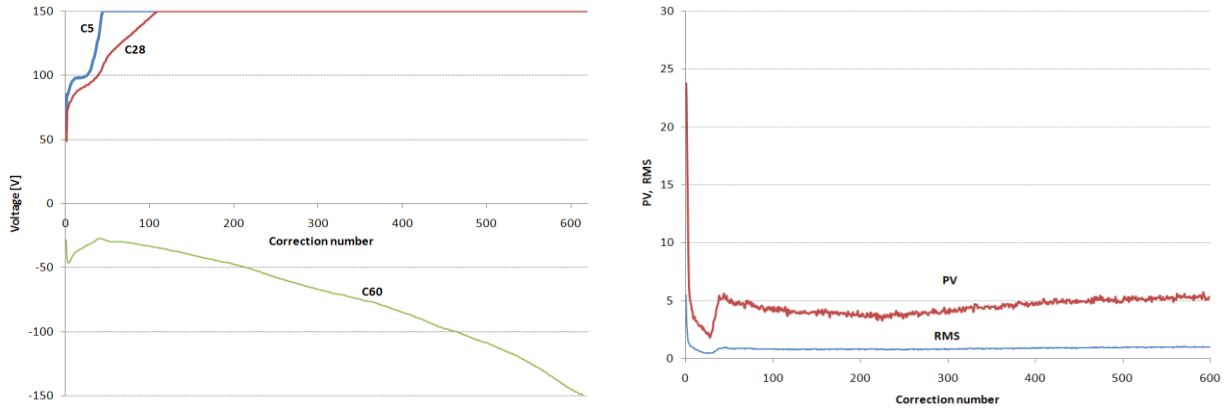

(a) Channel voltages (b) PV(peak-to-valley) and RMS values

Fig. 7. Channel voltages (a) and PV-RMS values (b) according to the number of corrections.

In this study, adaptive limited control techniques were devised to prevent the waste of voltage resources for correcting small non-meaningful wave-front distortions. The configured system does not apply voltages to a deformable mirror when the calculated correction environment meets one of the following three conditions: 1) if a current voltage RMS value of the DM actuators is less than a set threshold value (T_1), 2) if a difference RMS value of the voltage pattern between the current calculated actuator voltages and previously applied actuator voltages in a DM is less than a set threshold value (T_2), and 3) if the RMS value of the current wave-front distortion is less than a set threshold value (T_3).
In the experiment, the values (T_1, T_2, T_3) were calculated at the minimum RMS value of the residual wave-front distortion after repeated corrections for one wave-front distortion acquired from one position of the stopped phase plate. The threshold values were determined by equations nT_1, nT_2, and nT_3, where n is an integer value. The averaged threshold values acquired from ten positions of the stopped phase plate were used, and the value n was 2 ($2T_1$, $2T_2$, $2T_3$) in the experiment.
Experimental results using the three conditions for the correction limit in the same environment of Figs. 7 are shown in Figs. 8. The actuator voltages not consuming their voltage resources to correct for non-meaningful small distortions are shown in Fig. 8(a). Here, the voltages of three actuators, 5, 28 and 60, were not applied after the 16^{th} correction. Thus, the dynamic range of the system was increased for the correction of the next wave-front distortion.

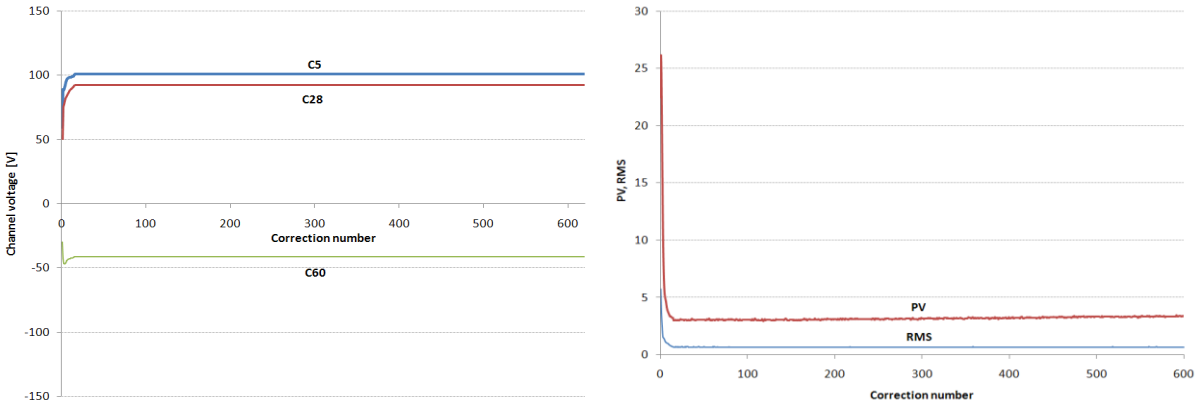

(a) Channel voltages (b) PV(peak-to-valley) and RMS values

Fig. 8. Channel voltages (a) and PV & RMS values (b) using stability control according to the number of corrections.

During correction, the wave-front spot shapes placed on the outer search grids are strongly distorted because of the generated steep slope in phase at the edge areas between the active outer actuators and non-active outer actuators. Here, the outer actuators placed on the outside of the used actuators were not applied because of their low performance. To reduce the steep slope generated in the outside edge area, an adaptive deformation using an interpolation voltage for the non-active outer actuators was adopted. For the experiment, the voltages on the non-active actuators were linearly interpolated from the voltages on the active neighboring actuators. This voltage interpolation improved the correction efficiency, as shown in Fig. 9. RMS values of the Zernike coefficients from 1 to 36 according to the correction numbers are shown in Fig. 9. Here, graph (a) shows the correction results using a fixed bias voltage for non-active outside actuators, and graph (b) shows the results using adaptive deformation based on linear interpolation voltages from non-active actuators.

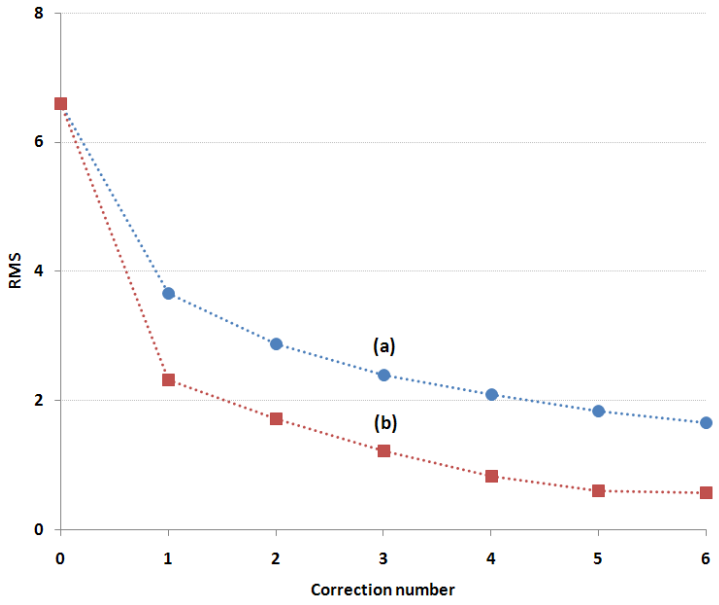

Fig. 9. RMS comparison of corrected wave-front using (a) conventionally- and (b) adaptively-controlled deformable mirrors.

The mechanical arrangement between the Shack-Hartmann WFS and the membrane DM can be distorted during long-term operation. The distortion can decrease the correction efficiency of the system and may cause a local voltage saturation of an actuator. The locally biased voltages of the DM actuators decrease the system performance

by reducing the dynamic correction range. Although users usually acquire a new influence function matrix (IFM) when the correction efficiency is low, the optimum correction efficiency is not fully recovered when the system is considerably distorted. Thus, the pre-recognition of the current arrangement distortion before a correction starts is useful for maintaining the optimum correction efficiency of the system because users can improve the system performance through a rearrangement based on the provided current information.
The distribution of eigenvalues from the center actuator of 31 is well balanced in the initial system alignment shown in Fig. 3. The distortion values of the X-axis and Y-axis are calculated according to equations (1) and (2) for the inspection of the balance information of the eigenvalues.

$$S_x = \left[\frac{\sum_{x=-4}^{4} \sum_{y=-4}^{4} V_{(x,y)} \times P_x}{\sum_{x=-4}^{4} \sum_{y=-4}^{4} V_{(x,y)}} \right] \tag{1}$$

$$S_y = \left[\frac{\sum_{x=-4}^{4} \sum_{y=-4}^{4} V_{(x,y)} \times P_y}{\sum_{x=-4}^{4} \sum_{y=-4}^{4} V_{(x,y)}} \right] \tag{2}$$

Here, V(x, y) is the eigenvalue mapped to a DM actuator position (x, y), and P_x and P_y are the positions of the X-axis and Y-axis notated in Fig. 3.
The distortion values of S_x and S_y of the initially well-arranged Fig. 3(a) were 0.067 and 0.097, respectively.
To see the effects of mechanical distortion, DM was moved toward the X-direction. The unbalance of the eigenvalue distribution is proportionally increased to the shifting values. The values of S_x and S_y from the shifted position of 105 ㎛ are 0.387 and 0.014, and the values are 0.517 and 0.135 from the shifted position of 210 ㎛. We can see that the unbalance of the eigenvalue distribution is proportionally increased to the shifting distortion values.
The Strehl ratios acquired from the repeated correction number for one fixed wave-front distortion are shown in Fig. 10. The correction results using zonal control and modal control are shown in Figs. 10(a) and 10(b), respectively. Here, notation 'A' means a non-shifted position, and notations 'B' and 'C' are shifted positions of 105 ㎛ and 210 ㎛ from the optimum correction position of 'A', respectively. The independent self-influence function acquired from each position was used in the experiment. As shown in this experiment, the correction performance according to the repeated correction number is decreased when the shifting distance is increased. The zonal control provided better correction results than the modal control results because sampling data of 77 points in the WFS were not enough to extract the precise modal modes, and the 36 used modal modes were also not enough to reconstruct a precise phase.

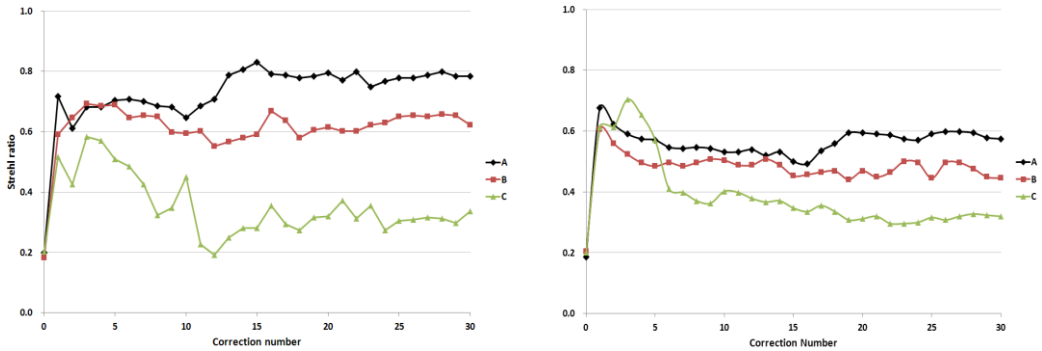

(a) Zonal control mode (b) Modal control mode

Fig. 10. Comparison of Strehl ratios acquired from repeated corrections in zonal and modal control modes.

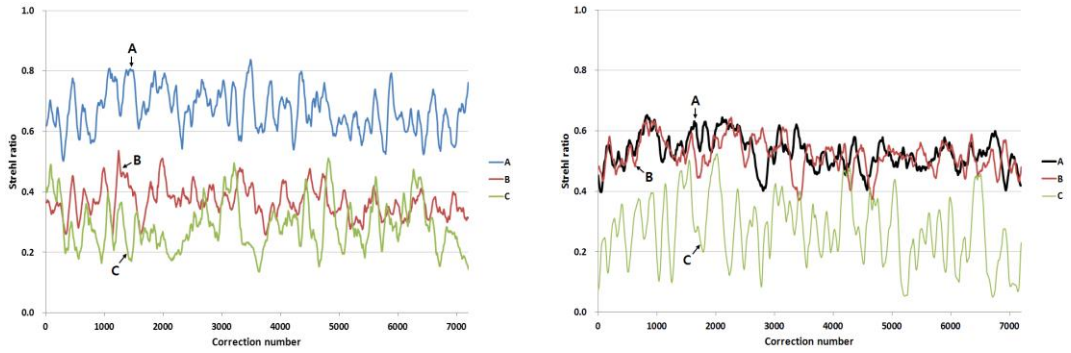

(a) Zonal control mode (b) Modal control mode

Fig. 11. Comparison of Sequential Strehl ratios acquired from a rotating phase plate using independent influence function matrices.

The Strehl ratios acquired from a rotating phase plate of one turn are shown in Fig. 11. The zonal and modal correction results are shown in Figs. 11(a) and 11(b), respectively. The average values for Figs. 11(a) and 11(b) are shown in Figs. 12(a) and 12(b), respectively. Here, an independent self-influence function was also used. The rotating speed of the phase plate was 3.7 mm/s, and the correction speed of the system was about 60 Hz. As shown in the experiments, the correction results were worse with an increase in the shifting distance.

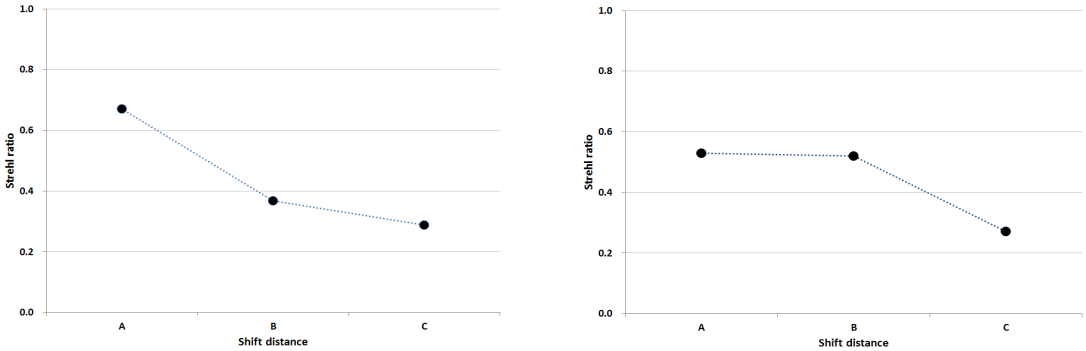

(a) Zonal control mode (b) Modal control mode

Fig. 12. Comparison of averaged Strehl ratios acquired from a rotating phase plate in the zonal and modal controls.

As a result of the experiments, the developed small-scale adaptive optics system using a cost-effective membrane deformable mirror stably improved the quality of the acquired images. The adopted limited control techniques based on the similarity of the voltage pattern, the RMS value of the voltage, and the RMS value of the wave-front distortion improved the system's stability by increasing the dynamic correction range of the configured system. In addition, an adaptive moving technique for the non-active actuators, which uses interpolated voltages, improved the correction efficiency. A pre-recognition process for checking the mechanical distortion of an adaptive optics system is a useful tool to provide efficient correction results over a long period of time. The process of confirming the eigenvalue balance is valuable to preventing a low-performance operation and improving the system stability by reducing the unexpected distortions caused by locally saturated voltages.

4. CONCLUSIONS

In this study, a cost-effective small-scale adaptive optics system using a membrane deformable mirror and a digital Shack-Hartmann wave-front sensor was built. The experimental results showed that the developed system can be stably operated by providing an improved Strehl ratio for the wave-front distortion. Stabilization techniques for the developed adaptive optics system for robust image acquisition were investigated in this study. The devised limited control techniques using the difference voltage pattern, voltage, and wave-front values efficiently improved the stability by increasing the dynamic correction range of the system. In addition, an adaptive deformation method for

the non-active outer actuators using interpolated voltages improved the correction efficiency of the system. In addition, the mechanical distortion effects between a WHS and a DM were studied, and a pre-recognition process for the distortion was devised to keep the optimal performance over a long period of time. The recognition technique for confirming a balanced work assignment among the DM actuators efficiently provided the arrangement distortion information. The process confirming the eigenvalue balance among the actuators is useful for improving the dynamic correction range in a closed-loop system.

5. REFERENCES

1. R. K. Tyson, *Principles of Adaptive Optics*, Academic Press, San Diego, 1991.
2. R. K. Tyson, *Adaptive Optics Engineering Handbook*, Marcel Dekker, New York, 2000.
3. M. E. Furber, *Optimal Design of Wavefront Sensors for Adaptive Optical Systems*, Ph.D dissertation, University of Connecticut, 1995.
4. Z. Wang, Z. Jin, J. Zheng, P. Wang, and Wei. Z, Zhang. J, *Wavefront correction of high-intensity fs laser beams by using closed-loop adaptive optics system*, Science in China Ser. G. Phys. 48(1), 2005, pp. 122-128.
5. O. Azucena, J. Crest, S. Kotadia, W. Sulivan, X. Tao, M. Reinig, D. Gavel, S. Olivier, and J. Kubby, *Adaptive optics wide-field microscopy using direct wavefront sensing* , Optics Letters. 36(6), 2011, pp. 825-827.
6. X. F. Zhang, and L. Q. Wang, *Improvement in the performance of solar adaptive optics*, Research in Astronomy and Astrophysics 14(4), 2014, pp.471-484.
7. R. J. Jawazadzki, A. G. Capps, D. Y. Kim, A. Panorgias, S. B. Stevenson, B. Hamann, and J. S. Warner, *Progress on Developing Adaptive Optics-Optical Coherence Tomography for In Vivo Retinal Imaging: Monitoring and Correction of Eye Motion Artifacts*, IEEE J. of Selected Topics in Quantum Electronics 20(2), 2014, pp.322-333.
8. Y. Li, *Imaging the Foveal Cone Mosaic with a MEMS-based Adaptive Optics Scanning Laser Ophthalmoscope*, Ph. D dissertation (Univ. of California), 2010.
9. D. X. Hammer, R. D. Ferguson, C. E. Bigelow, N. V. Iftimia, T. E. Ustun, and S. A. Burns, *Adaptive optics scanning laser ophthalmoscope for stabilized retinal imaging*, Optics Express, 14(8), 2006, pp.3354-3367.
10. M. Nagashima, J. J. Kim, B. Agrawal, *Comparison of the Performance of Modal Control Schemes for an Adaptive Optics and Analysis of the Effect of Actuator Limitations*, DEPS Beam Control Conference, Broomfield, CO, 2012.
11. Scott M. Jobling, *Adaptive Optics for Improved Mode-Coupling Efficiencies*, Master's thesis, University of Illinois, 2008.